Polyhedron 180 (2020) 114424

Contents lists available at ScienceDirect

Polyhedron

journal homepage: www.elsevier.com/locate/poly

Synthesis and characterization of $Sm_2(MoO_4)_3$, $Sm_2(MoO_4)_3$/GO and $Sm_2(MoO_4)_3/C_3N_4$ nanostructures for improved photocatalytic performance and their anti-cancer the MCF-7 cells

Shahrzad Behvandi [a], Ali Sobhani-Nasab [b,c,*], Mohammad Ali Karimi [a], Esmail Sohouli [d], MeisamSadeghpour Karimi [e], Mohammad Reza Ganjali [e,f], Farhad Ahmadi [g,h], Mehdi Rahimi-Nasrabadi [i,j,*]

[a] Department of Chemistry, Payame Noor University, Tehran, Iran
[b] Social Determinants of Health (SDH) Research Center, Kashan University of Medical Sciences, Kashan, Iran
[c] Core Research Lab, Kashan University of Medical Sciences, Kashan, Iran
[d] Young Researchers and Elite Club, Science and Research Branch, Islamic Azad University, Tehran, Iran
[e] Center of Excellence in Electrochemistry, Faculty of Chemistry, University of Tehran, Tehran
[f] Biosensor Research Center, Endocrinology & Metabolism Molecular Cellular Sciences Institute, Tehran University of Medical Sciences, Tehran, Iran
[g] Physiology Research Center, Iran University of Medical Sciences, Tehran 1449614535, Iran
[h] Department of Medicinal Chemistry, School of Pharmacy-International Campus, Iran University of Medical Sciences, Tehran, Iran
[i] Chemical Injuries Research Center, Systems Biology and Poisonings Institute, Baqiyatallah University of Medical Sciences, Tehran, Iran
[j] Faculty of Pharmacy, Baqiyatallah University of Medical Sciences, Tehran, Iran

ARTICLE INFO

Article history:
Received 1 October 2019
Accepted 29 January 2020
Available online 1 February 2020

Keywords:
Samarium molybdate
Graphene oxide
Carbon nitride
Nanocomposite
Photo-degradation
Cytotoxicity

ABSTRACT

Samarium molybdate nanoparticles ($Sm_2(MoO_4)_3$) were prepared through a hydrothermal procedure and were used to form various composites with graphene oxide (GO) and carbon nitride (C_3N_4). The changes in the dimensions and morphology of the products were prepared using template agents like cetyltrimethyl ammonium bromide (CTAB), Sodium dodecyl sulfate (SDS) (≥90%), Triton X-100 (90%), Polyvinyl alcohol (95%), Ethylene glycol (≥99%), and polyvinylpyrrolidone (PVP). DRS analysis indicated band gap for the $Sm_2(MoO_4)$, $Sm_2(MoO_4)_3$/GO, and $Sm_2(MoO_4)_3/C_3N_4$ as 3.75, 3.15, and 3.4 respectively. The characteristics of the prepared nanostructures were studied through X-ray diffraction (XRD), energy dispersive X-ray (EDX), and scanning electron microscopy (SEM). Finally, the activity of the prepared $Sm_2(MoO_4)_3$ as photo-catalysts for the degradation of different organic dyes such as methyl orange (MO), methylene blue (MB), and rhodamine B (Rh B) was evaluated. The photocatalytic property of $Sm_2(MoO_4)_3/C_3N_4$ and $Sm_2(MoO_4)_3$/GO for the degradation of MO, was obtained. Based on the empirical data $Sm_2(MoO_4)_3/C_3N_4$ had the strongest photodegradation effect as compared to the other compounds tested after around 40 min. BET analysis revealed that the specific surface area of the $Sm_2(MoO_4)_3$ nanocomposite prepared using C_3N_4 is 15 times that of in the absence of C_3N_4. Also, the cytotoxicity of synthesized samples was evaluated using MTT assay against human cell lines MCF-7 (cancer), and its IC50 was about 125 mg/L.

© 2020 Elsevier Ltd. All rights reserved.

1. Introduction

Dyes are one of the most important chemicals that easily enter the environment due to the increasing the industrial activity and ignoring required environment [1]. In the meantime, textile dyes are the most widely used chemicals that have high consumption [2]. Every year, ten thousand different dyes are supplied in an amount of 700 thousand tons, and can finally find their way into water supplies [3].Precise data on the evacuation of these colored materials entered to the environment is not available. However, one of the major challenges, which engineers and environmental experts have to deal with, is the removal of these materials and pollutants from the environment [4].Therefore, different ways have been used to solve this problem [5–11].

On the hand cancer, one of the most important health problems, may lead to disability and mortality in the world. Among various cancers, pancreatic cancer, show a high incidence worldwide. It has been shown that new therapeutic approaches along with the current therapeutic tools are needed [12–15]. In the past years,

* Corresponding authors at: Social Determinants of Health (SDH) Research Center, Kashan University of Medical Sciences, Kashan, Iran (A. Sobhani-Nasab). Chemical Injuries Research Center, Systems Biology and Poisonings Institute, Baqiyatallah University of Medical Sciences, Tehran, Iran (M. Rahimi-Nasrabadi).
E-mail addresses: Ali.sobhaninasab@gmail.com (A. Sobhani-Nasab), Rahiminasrabadi@gmail.com (M. Rahimi-Nasrabadi).

https://doi.org/10.1016/j.poly.2020.114424
0277-5387/© 2020 Elsevier Ltd. All rights reserved.

photocatalytic materials have been considered to be the most studied fields, which can destroy harmful contaminant from the water [16–24]. Meanwhile, the photocatalytic degradation of pollutants is of great interest due to its simplicity, good performance, excellent efficiency, and easy operation under sunlight and environmental conditions [24–31]. Semiconductor compounds such as TiO_2, Nd_2O_3, ZnO and their nanocomposites which have photocatalytic properties are at the top of photocatalyst materials [32–35]. The extensive applicability of photocatalytic degradation has led to various compounds which have been studied in this area [36–40]. Lanthanides are f-block elements, and the nature of the f-orbital and the possibility of their overlapping with donor atoms orbitals in ligands allow the creation of trivalent lanthanides complexes with high coordination number and different spatial orientations. Trivalent lanthanide ions have high scientific and industrial applications. Recently, they have also been used in photocatalytic degradation of various pollutants [41–48]. Carbon materials have different applications in various fields due to their suitable chemical properties and high conductivity. Graphene, nanotube as well as carbon nanofiber are the carbon-based materials, which are what have made the chemistry so beautiful [49–51]. Graphene is a 2D sheet composed of carbon, in which the sp^2 atoms are located in a hexagonal honeycomb configuration [52]. Extraordinary properties of graphene including high density of electric current, chemical inertia, high thermal conductivity, optical transport and supernatural hydrophobicity in nanometer scale have attracted great attention [52]. Nowadays, graphene (GO) and its nanocomposites with semiconductors and other compounds have photocatalytic application [53–56]. In recent research, for the first time our research team synthesized $Sm_2(MoO_4)_3$ nanoparticles with various templates by the hydrothermal method and used their nanocomposite with GO and carbon nitride (C_3N_4) for degradation of dye pollutants. In addition, some parameters affecting photocatalytic degradation of pollutants as well as kinetics performance of photocatalytic degradation of pollutants were investigated in water samples.

2. Experimental

2.1. Materials and physical measurements

≥99.9% $Sm(NO_3)_3{\cdot}6H_2O$, ≥99.5% $Na_2MO_4{\cdot}2H_2O$, ≥99% CTAB, ≥90% SDS, 90% Triton X-100, 95% polyvinyl alcohol, ≥99% ethylene glycol, 99% polyvinylpyrrolidone, 98% H_2SO_4, 99% H_3PO_4, 30% H_2O_2, ≥99% $KMnO_4$, melamine, and the rest of chemicals and solvents were procured from Merck and Sigma-Aldrich companies and were used as received.

Size and morphology evaluations were performed using a TESCAN-Vega 3 scanning electron microscope (SEM). Crystalline structures of the samples were studied on a Rigaku D/max 2500 V X-ray diffraction spectrometer (XRD). Fourier transform infrared (FT-IR) spectroscopy tests were conducted on Brucker Equinox 55 IR spectrophotometer and the UV–Vis diffuse reflectance spectra (DRS) were recorded using an Avantes Avaspec-2048-TEC instrument. The photodegradation activities of the prepared materials were evaluated using methyl orange (MO), methylene blue (MB), and rhodamine B (Rh B) and the correspondent concentration were made using a Shimadzu, UV-1800 UV–Vis spectrophotometer (Japan).

2.2. Preparation of graphene oxide

Typically, 1 g of graphite powder was weighed and transferred into a beaker. Next 120 ml of H_2SO_4 and 15 ml H_3PO_4 and added to the beaker under stirring in ambient temperature for 16 h. After this step, the reaction mixture was moved to an ice bath. After a short time, about 6 g of potassium permanganate was slowly added to the reaction mixture, just before the container was transferred to a 30–40 °C oil bath, where the solution became green. Then, the temperature of the oil bath was set at 50 °C and the solution was kept at stirring at this temperature for 12 h. Next, 1 ml of a 30% solution of H_2O_2 in 300 ml water was gradually added to this mixture, to yield a yellowish brown solution. This product was separated by centrifuging and repeatedly washed with deionized water, 10% HCl, and ethanol. The product was finally rinsed with distilled water until neutral pH was reached and then the product was dried at 50 °C in an oven for 24 h (Scheme 1).

2.3. Preparation of C_3N_4

The thermal decomposition of melamine was used to synthesize C_3N_4. For this purpose, 5 g of melamine was heated from ambient temperature to 500 °C at a rate of 10 °C/min in an electric furnace for 2 h followed by another heating step at 550 °C for 2 h and a final cooling at room temperature. The resulting product was eventually grounded using a mortar and once more heated to 550 °C and kept at this temperature for 4 h.

2.4. Preparation of samarium molybdate nanoparticles

$Sm_2(MoO_4)_3$ nanoparticles were formed by means of a hydrothermal reaction using solutions of the corresponding cation and anion. For this purpose, aqueous solution of samarium nitrate and sodium molybdate with concentration of 0.05 M was prepared. In different experiments, 0.2 g of each template, (i.e. CTAB, SDS, Triton X-100, PVA, PEG or PVP) was mixed with the anion solution as a template in separate steps. Using a peristaltic pump the samarium solution was then added to that of molybdate at 10 ml/min, while the receiving solution was stirred before the resulting suspension was transferred to an autoclave with an inner teflon coating and the system was moved to an electric oven and kept at 180 °C for 18 h. Once the reaction was completed, the resulting solid product was isolated by centrifuging and repeatedly washed with water and ethanol and then kept at 80 °C for 4 h to dry. The conditions and procedures of the synthesis of $Sm_2(MoO_4)_3$ were presented in Table 1.

2.5. Synthesis of $Sm_2(MoO_4)_3$/GO

$Sm_2(MoO_4)_3$/GO composite was synthesized with various mass ratios of $Sm_2(MoO_4)_3$ to GO. For that reason, this composite with 1: 1, 10: 1, and 20: 1 mass ratios were synthesized according to the following method. The known amounts of GO according to Table 2 was dispersed in 10 ml of distilled water by sonication for 30 min. Up to 0.36 g of Na_2MO_4 was dissolved in 5 ml distilled water and this solution was mixed with graphene oxide under sonication for 15 min. Next, 0.44 g of $Sm(NO_3)_3{\cdot}6H_2O$ was dissolved in an independent volume of distilled water (10 ml) and gradually added to the mixture of GO and the Na_2MO_4 solution using a peristaltic pump. Afterwards, the reaction mixture was poured into an autoclave heated at 180 °C in an electric oven for 18 h. The resultant precipitate was isolated by centrifuge, and cleaned in the same fashion as described before and then dried at 80 °C for 4 h.

2.6. Preparation of $Sm_2(MoO_4)_3/C_3N_4$ nanocomposite

$Sm_2(MoO_4)_3/C_3N_4$ composite was synthesized in different mass ratios of $Sm_2(MoO_4)_3$ to C_3N_4.To do so, the composite was synthesized in the 10: 1 and 30: 1 mass ratios using the following method. The specified amount of carbon nitride given in Table 3was weighed and dispersed in a beaker containing 10 ml of water by sonication for 30 min. Next, 0.36 g of Na_2MO_4 was dis-

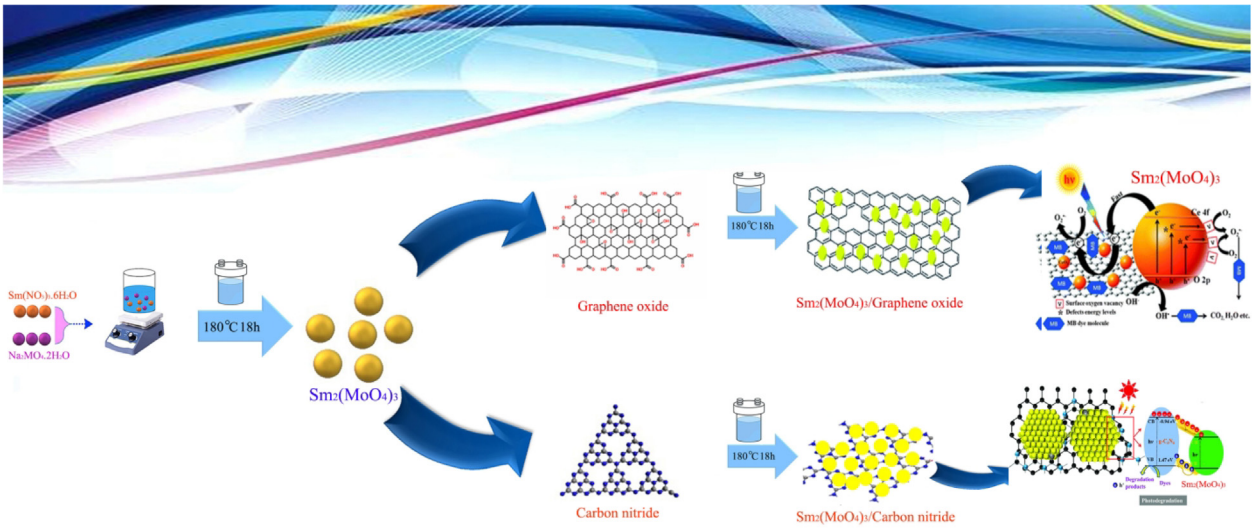

Scheme 1. Schematic mechanism for the synthesis of $Sm_2(MoO_4)_3$, $Sm_2(MoO_4)_3$/GO and $Sm_2(MoO_4)_3/C_3N_4$ and its different application.

Table 1
Synthesis of $Sm_2(MoO_4)_3$nanoparticles.

Test number	Samarium solution concentration (M)	Molar ratio Sm^{3+}:MoO_4^{2-}	Reaction temperature (° C)	Reaction time (h)	Template Type
1	0.05	1:1	180	18	–
2	0.05	1:1	180	18	CTAB
3	0.05	1:1	180	18	SDS
4	0.05	1:1	180	18	Triton X-100
5	0.05	1:1	180	18	PVA
6	0.05	1:1	180	18	PVP
7	0.05	1:1	180	18	PEG

Table 2
Synthesis of $Sm_2(MoO_4)_3$/GO Composite.

Test number	Samarium nitrate (g)	Sodium molybdate (g)	GO (g)	Mass ratio GO:$Sm_2(MoO_4)_3$
1	0.44	0.36	0.36	1:1
2	0.44	0.36	0.36	1:10
3	0.44	0.36	0.018	1:20

solved in 5 ml of water and added to C_3N_4 solution by sonication for 15 min. Subsequently, up to 0.44 g $Sm(NO_3)_3$ was dissolved in 10 ml of water. This solution was gradually added to that of sodium molybdate and C_3N_4 using a peristaltic pump. Subsequently, they were transferred to an autoclave, and heated at 180 °C for 18 h, and repeatedly washed with water and ethanol, and then dried for 4 h at 80 °C.

2.7. Photocatalytic activity

The photocatalytic effects of the synthesized nanostructures were in the UV-induced degradation of model dyes. The photoreactor was a double-walled Pyrex photo-reactor with a lamp located in the middle. The light source was a UV high pressure Hg lamp (240 W,$\lambda > 280$nm).Suspension of the reaction was prepared by addition of photocatalyst to 500 ml of a 5 mg/l solution of the dye in water. The reaction system was performed under thermostatic conditions at 25 °C, using a cooling system.

Prior to the onset of UV radiation, the mixture was stirred in the reactor for 20 min (in the absence of light) to reach an absorbance/absorbance equilibrium. Then, the solution of reaction, photocatalyst, and dye model were then subjected to UV light from the Hg lamp, while the solution was being aerated with a pump. Before and during the reaction (at known intervals) samples of the reaction mixture were taken, centrifuged, and studied using UV–Vis absorption to determine the concentration of the model dye. To measure the degradation and efficiency of organic species and to determine the λ_{max}, the absorption of dye should be measured in the absence of photocatalyst. Then the value of absorbance (A_0) has to be recorded at λ_{max}. With the aid of the calibration curve,

Table 3
The synthesis conditions of $Sm_2(MoO_4)_3/C_3N_4$ Composite.

Test number	Samarium nitrate (g)	Sodium molybdate (g)	C_3N_4 (g)	Mass ratio C_3N_4:$Sm_2(MoO_4)_3$
1	0.44	0.36	0.036	1:10
2	0.44	0.36	0.012	1:30

C_0 and C were determined and the absorbance (A) is read after adding of the photocatalyst to the dye solution, stirring for different times and centrifugation for 20 min, and the percentage of degradation was obtained through the following relation. R = (C_0 − C) (Eq. 1) degradation efficiency. The concentration of dye samples at different time intervals is determined by using the Lambert equation:

$$A = \varepsilon bc \quad (1)$$

In which c is the concentration of the test sample, A is the absorption, £ is the molar absorption coefficient, b expresses the cell length. Given that b and £ are constant during a specific experiment one can follow the formula below:

$$A/A_0 = C/C_0 \quad (2)$$

The percentage of dye degradation at each stage of the experiment is also derived from the No.1 relation equation.

The kinetics of the reactions are evaluated using the Langmuir kinetic (Langmuir-Hinshelwood), which is a common method for degradation of the dilute solution of organic pollutants.

2.8. Cell culture

Panc1 cell lines were the curtsey of the National Cell Bank of Iran (NCBI, Tehran) and were grown in a RPMI 1640 medium (Gibco) also containing 10% (v/v) Fetal Bovine Serum (FBS), 100 IU/ml of penicillin and 100 µg/od streptomycin. The next procedure was incubation and preservation of cells in the atmosphere with a temperature of 37 °C and 5% CO_2. As soon as confluence got to 85%, we rinsed cells with pure RPMIq and gathered via 0.25% trypsin/EDTA solution (Sigma). We performed test 3 times each.

2.9. MTT assay

MTT assay was used to evaluate the cytotoxicity of the extract on MCF-7 cells. The cells were collected and plated at 10^4 cells/well in a nunc 96-well plate. Then, each cell was treated with varying concentrations of nanocomposites (2, 1, 0.5, 0.25, 0.125, 0.063, 0.0315, 0.0157 mg/ml). For 1 and 2 days we incubated the microplateat 37 °C and 5% CO_2. Then, we discarded supernatants and added 100 µL of the DMSO to every well, and incubated plates for 20 min. Eventually, we used ELISA plate reader at ƛ = 570 nm to observe cytotoxicity. The amount of cytotoxicity and viability, in terms of percentage, could be achieved through the following relation [27]:

$$\text{Cytotoxicity}\,(\%) = (1 - \text{Mean absorbance of toxicant} / \text{Mean absorbance of negative control}) \times 100 \quad (3)$$

3. Results and discussion

3.1. SEM analysis of the samples

SEM images of synthesized GO and carbon nitride is have been shown in Fig. 1. As shown in the figure, the synthesized GO has spread layers and their thicknesses lie between one to several layers and synthesized C_3N_4 has large and layered plates. The SEM images of the synthesized $Sm_2(MoO_4)_3$ nanocomposites in accordance with the conditions has been reported in Table 1. $Sm_2(MoO_4)_3$ was synthesized by hydrothermal method without adding the template (Fig. 2a) in the form of imbricated and lamellar, and the thickness of the layers was 30–60 nm. With addition of CTAB to the reaction, the particles changed in terms of morphology to thin plates with thicknesses of around 20 nm or to 50–130 nm particles (Fig. 2b). In the presence of SDS (Fig. 2c), the particles underwent total morphology changes and turned to 30–50 nm particles, whereas in the presence of Triton X-100 (Fig. 2d) single layers of around 10–30 nm in thickness were obtained. When using PVA (Fig. 2e), shapeless nanoparticles with the size of 20–200 nm were formed, while in the presence of PVP (Fig. 2f), the particles were synthesized in bean form with 500 nm diameter. By addition of PEG to the reactants like PVP (Fig. 2g) the bean-formed shape particles with 500 nm size was obtained. As shown in the figures, the synthesized particles have different morphologies and particle sizes. SEM images of the composite prepared from $Sm_2(MoO_4)_3$/GO according to Table 3 are shown in Fig. 3a and c. Increasing the $Sm_2(MoO_4)_3$ content led to the formation of $Sm_2(MoO_4)_3$ flakes. Also SEM composite images prepared from $Sm_2(MoO_4)_3/C_3N_4$were presented in Table 3 in Fig. 3e-d.

3.2. XRD spectrum of synthesized samarium molybdate and its nanocomposits

The XRD pattern of the $Sm_2(MoO_4)_3$ nanoparticles synthesized by hydrothermal method is shown in Fig. 4a. As is clear in the figure, The spectrum of the pure of $Sm_2(MoO_4)_3$ sample contains a set

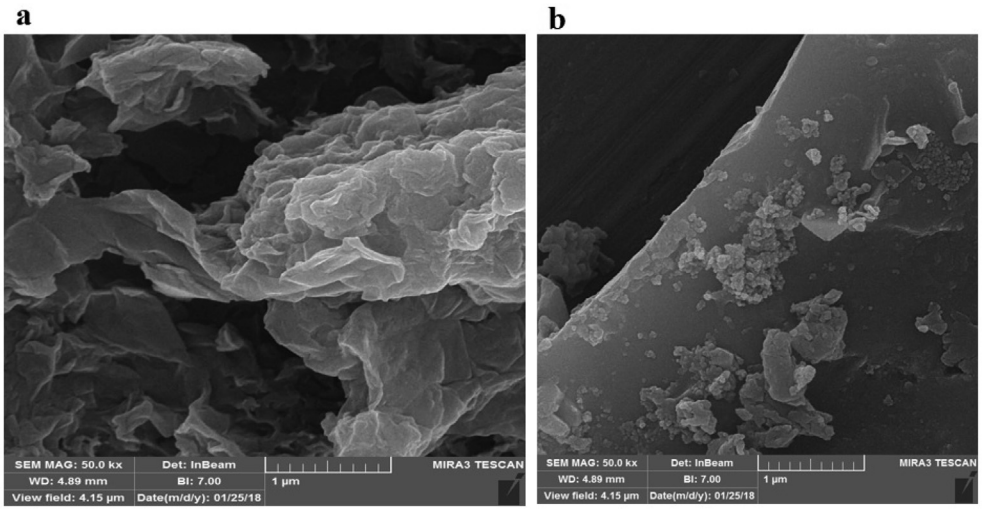

Fig. 1. SEM images of the synthesized a) GO and b) C_3N_4.

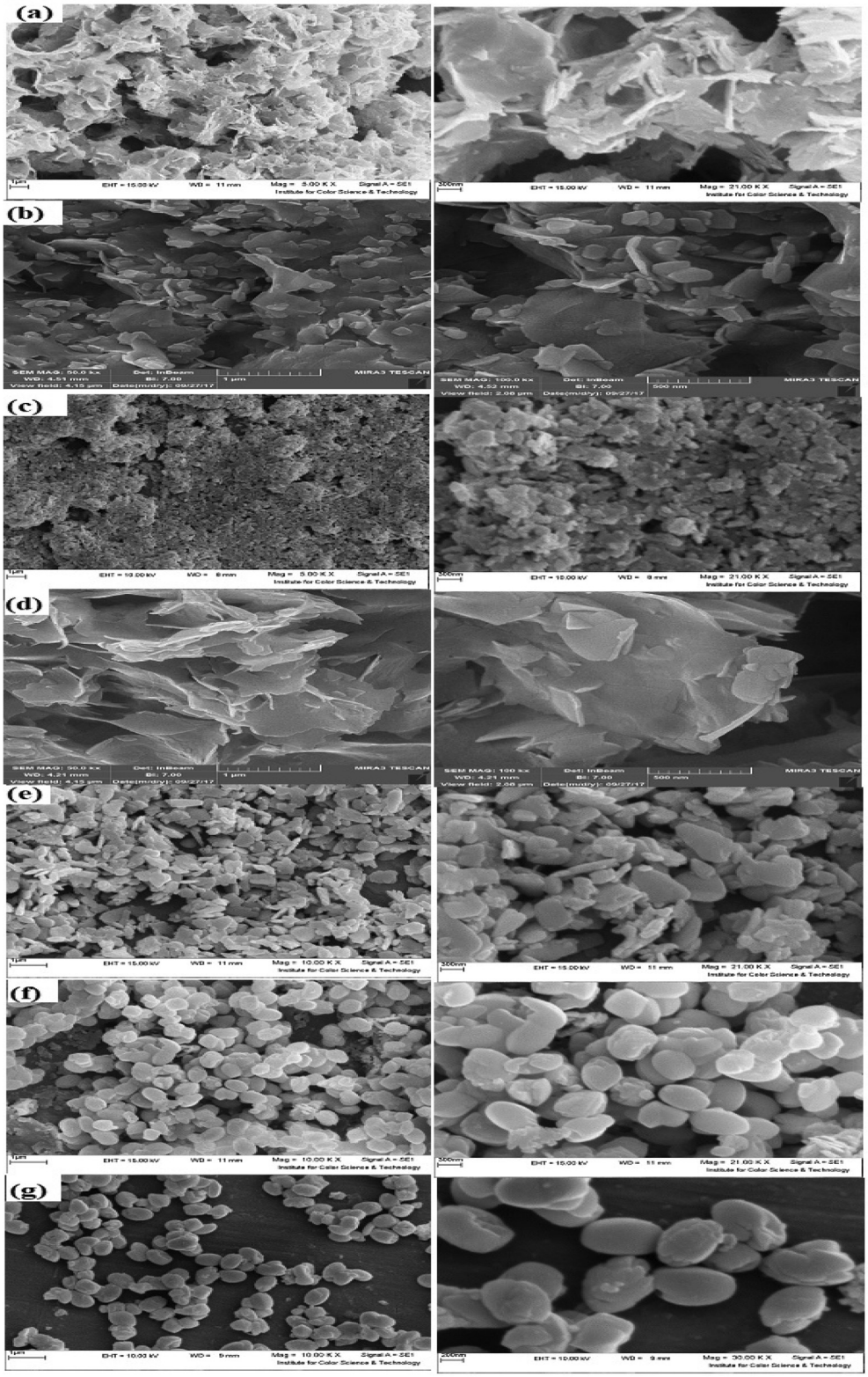

Fig. 2. SEM images of nanostructures of Samarium Molybdates synthesized with template, a) without template, b) CTAB, c) SDS, d) Triton X-100, e) PVA, f) PVP and g) PEG.

of peaks at 28.55° ((1 1 1) line), 34.12° ((2 2 1) line), and 46.41° ((1 0 0) line). These fully supported the presence of cubic $Sm_2(MoO_4)_3$ (JCPDS026-0990) and the cell parameters were calculated to be a = b = c = 10.4060 Å. As a result, the samarium molybdate nanoparticles are prepared with the high purity and crystallinity [5]. Fig. 4b shows the XRD pattern obtained for $Sm_2(MoO_4)_3$/GO, clearly indicating that a spectral pattern which is fully consistent with the standard sample of $Sm_2(MoO_4)_3$ with the reference code 034-0512 and graphene with reference code 01-075-2078, reflecting high crystallinity and purity. Fig. 4c illustrates the XRD pattern recorded for $Sm_2(MoO_4)_3/C_3N_4$, which is once again fully consistent with the standard sample of $Sm_2(MoO_4)_3$ and C_3N_4 (with respec-

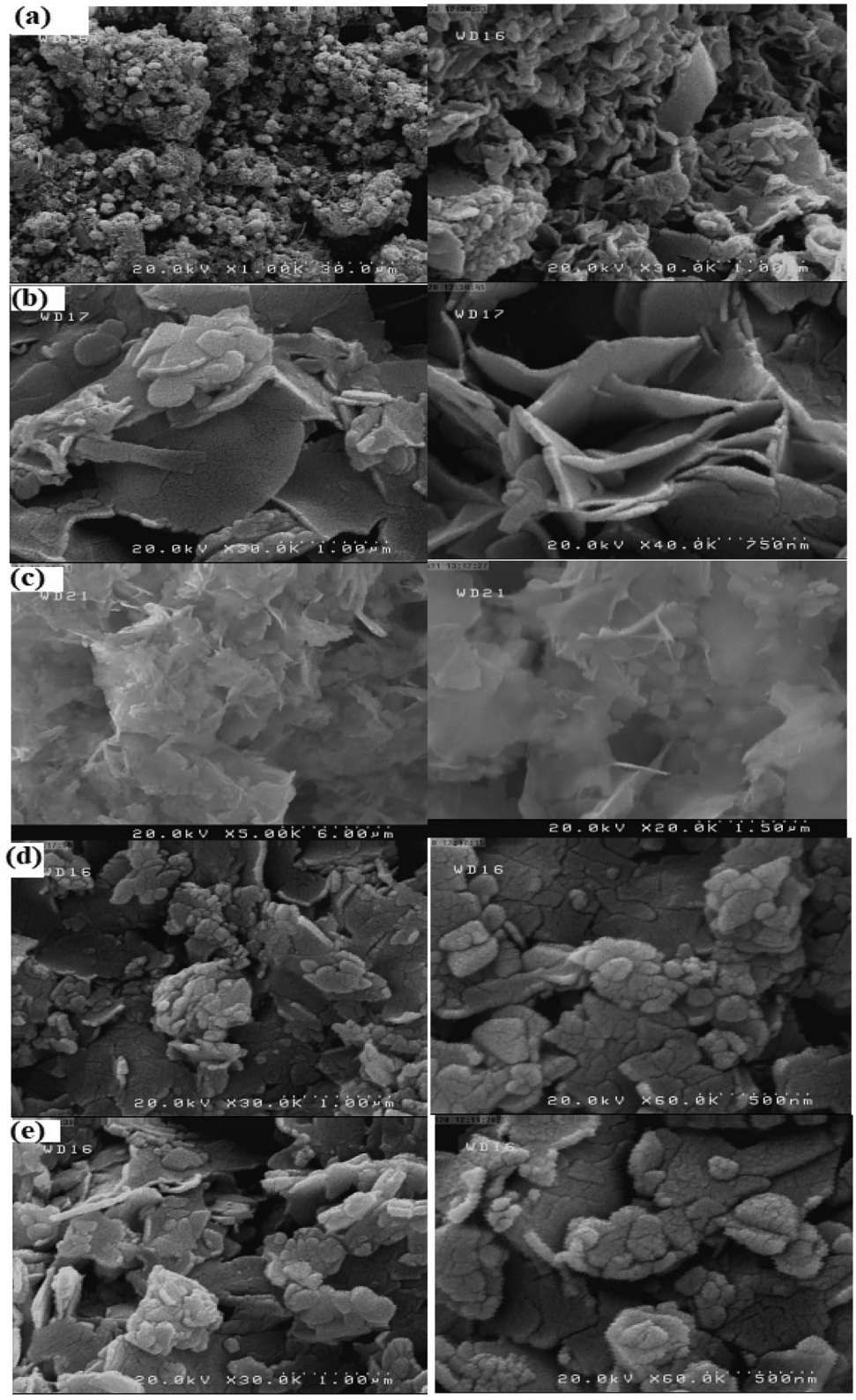

Fig. 3. SEM images of samarium molybdate/graphene composite with a samarium molybdate to graphene oxide mass ratio a) 1: 1, b) 10: 1, c) 20: 1, d and e) molybdate composite/carbon nitride oxide with a mass ratio of samarium molybdate to carbon nitride 10: 1 and 30: 1.

tive reference codes: 034-0512, 050-1512). This reflects high crystallinity and purity. The reaction mechanism in the presence of $Sm_2(MoO_4)_3$ nanoparticles is:

$$3Na_2MoO_4.2H_2O + (capping\ agent) \rightarrow 6Na^+ + 3MoO_4^{2-} + (capping\ agent) + 6H_2O \quad (4)$$

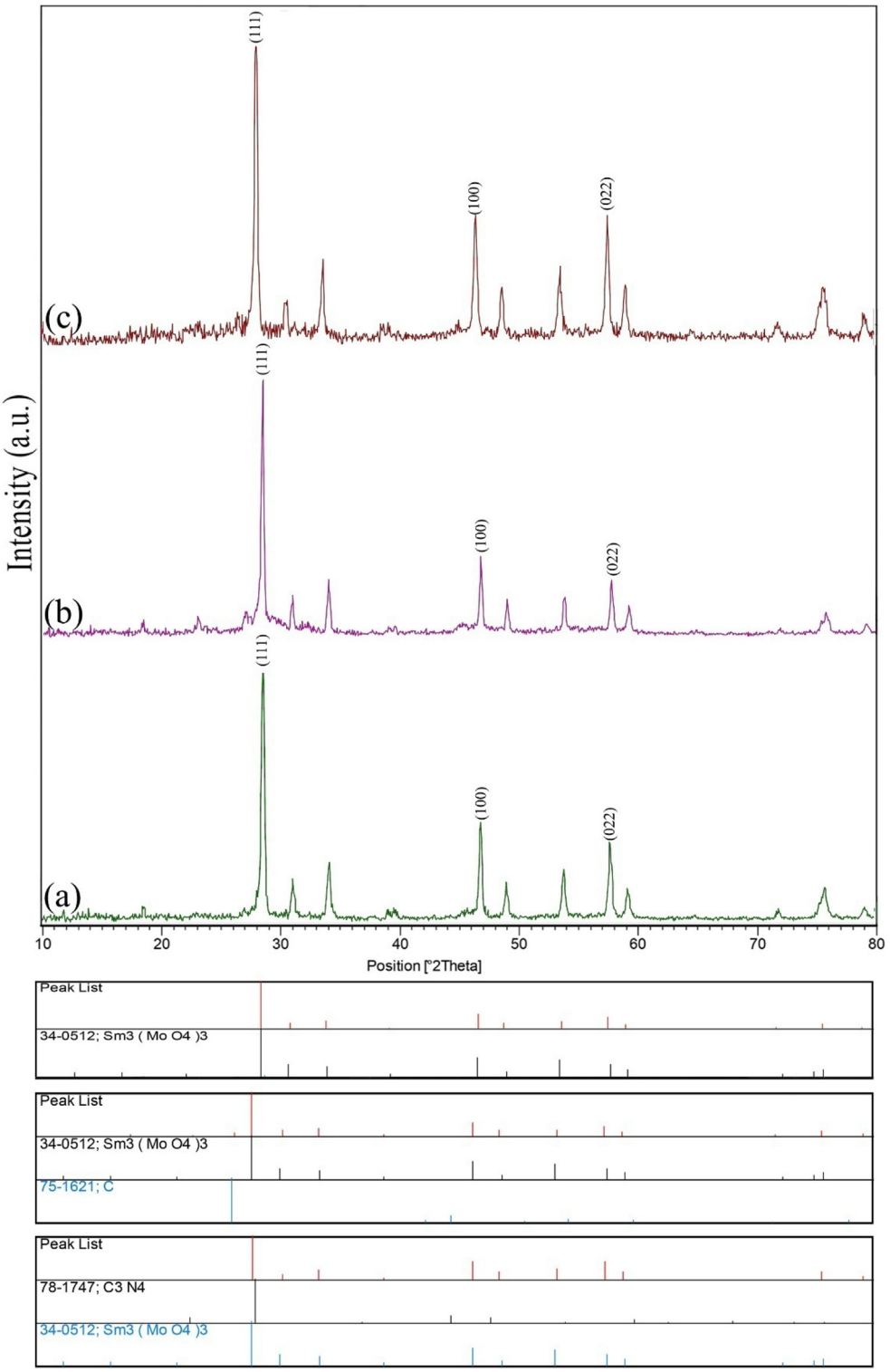

Fig. 4. a). The XRD Pattern of $Sm_2(MoO_4)_3$b) $Sm_2(MoO_4)_3$/GO composite synthesized by hydrothermal method and c) $Sm_2(MoO_4)_3/C_3N_4$ composite.

$$2Sm(NO_3)_3.6H_2O \rightarrow 2Sm^{3+} + 6NO_3^- + 12H_2O \quad (5)$$

$$6Na^+ + 6NO_3^- \rightarrow 6NaNO_3 \quad (6)$$

$$6Yb^{3+} + 2MoO_3^{2-} + \Delta T, \rho \uparrow \rightarrow Sm_2(MoO_4)_3 \quad (7)$$

$$3Na_2MoO_4.2H_2O + 2Sm(NO_3)_3.6H_2O + \Delta T, \rho \uparrow + (capping\ agent) \rightarrow Sm_2(MoO_4)_3 + 6NaNO_3 + (capping\ agent) + 20H_2O \quad (8)$$

3.3. FTIR spectrum of samarium molybdate samples

The FTIR spectrum of the synthesized samples was studied. Fig. 5 shows the results for $Sm_2(MoO_4)_3$ and those of composites with different ratios of GO. Fig. 4b shows the spectra obtained for composite with different ratios of C_3N_4. Clearly, any increase in the ratio of GO, decreases the intensity of peak. The absorption peaks at 940, 826, and 715 cm^{-1} regions also correspond to the tensile vibration of Mo-O bands [47].

3.4. DRS spectra

The DRS spectra and the Tauc's diagrams for $Sm_2(MoO_4)_3$ and its composite with GO and C_3N_4 can be seen in Fig. 6. The estimated band gap energy for the $Sm_2(MoO_4)$ and $Sm_2(MoO_4)_3$ composites, GO and C_3N_4 are 3.75, 3.15, 3.4, respectively. It can be concluded that the red shift in the case of the $Sm_2(MoO_4)_3$ nanocomposites leads to enhanced photocatalytic properties under light. Our findings showed that the red shift in the nanocomposites can increase photocatalytic properties. When $Sm_2(MoO_4)$ nanoparticles are dispersed on grapheme oxide, a significant change is measured in the absorption spectrum. The red shift of the absorption transition to higher wavelength may be due to the successful interaction of $Sm_2(MoO_4)$ nanoparticles with the grapheme oxide and carbon nitride. The characteristic features of absorption spectrum indicate that nanocomposite is in the conduction state.

3.5. Photocatalytic activity of $Sm_2(MoO_4)_3$ and the nature of the dyes

To study the relation between the photocatalytic properties of $Sm_2(MoO_4)_3$ and the type of the dyes, MO, MB, and RB solutions were prepared and tested. Fig. 7a-c shows the photocatalytic activity of $Sm_2(MoO_4)_3$ synthesized without a template in photocatalytic removal of three dye models. As are evident in these figures, the use of $Sm_2(MoO_4)_3$ as a photocatalyst has led to the dye degradation and the reduction of their initial concentration. The 0.05 g of $Sm_2(MoO_4)_3$ was dispersed in 2 ml distilled water. The photocatalyst was then reacted separately with the solution of three dyes (5 ppm) and the results for the removal of photocatalyst of three dyes were given in the following figure. Fig. 6d shows the photocatalytic degradation of the three dyes of methyl orange, methylene blue and rhodamine B by $Sm_2(MoO_4)$. It is evident that 99, 93 and 91% of them are degraded during the 60 min, respectively. According to these data, it is clear that the methyl orange is a suitable dye to study the photocatalytic activity of the catalyst and the remaining parameters will be investigated for this dye.

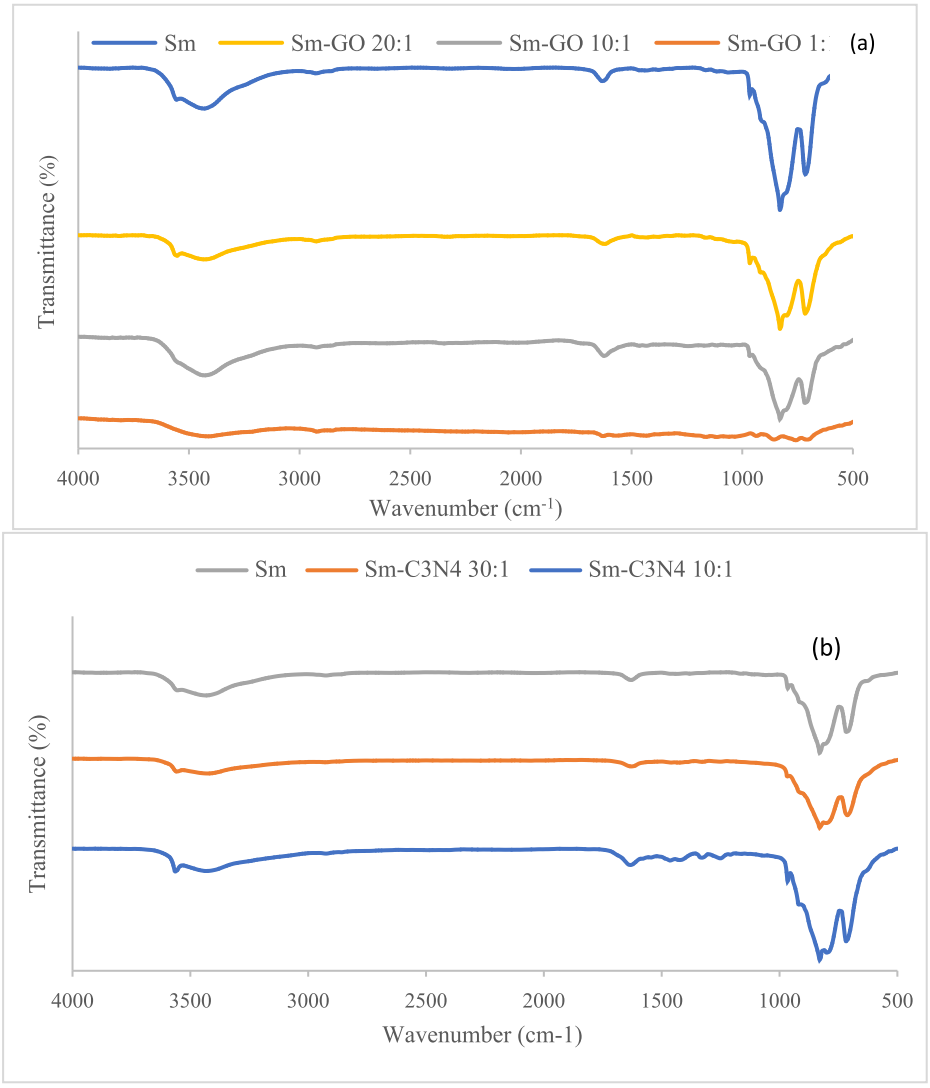

Fig. 5. The FTIR spectrum of $Sm_2(MoO_4)_3$ with its composites a) GO and (b C_3N_4.

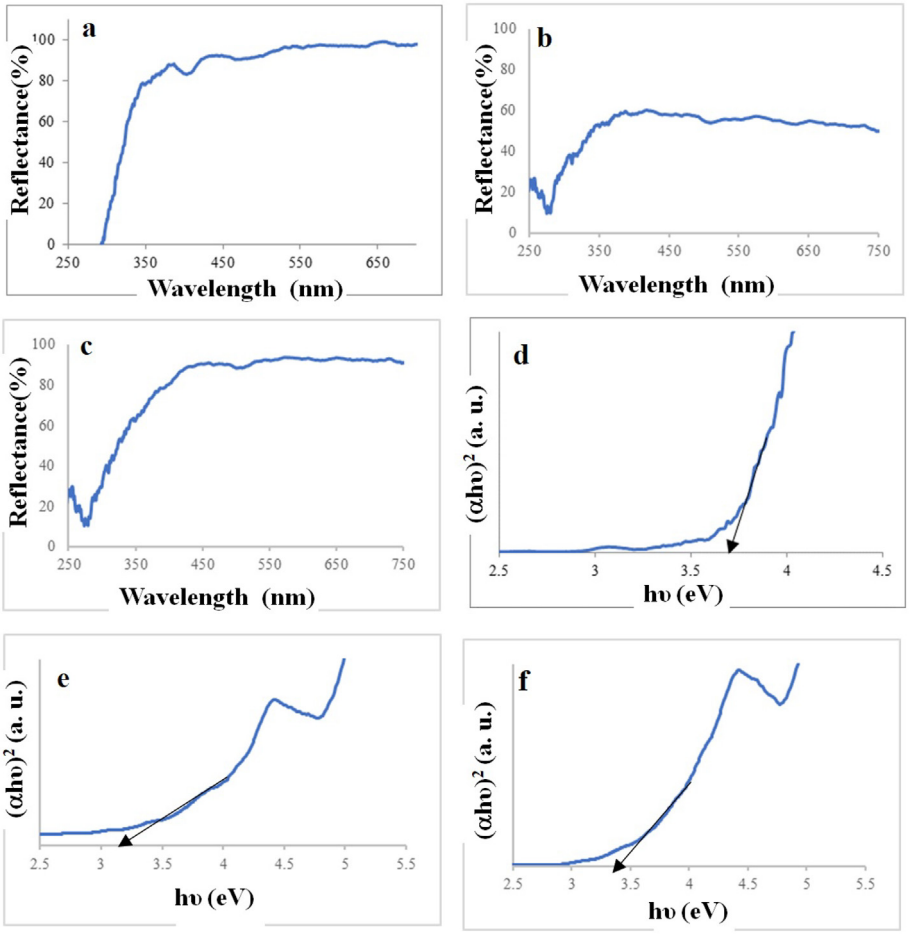

Fig. 6. DRS of as-synthesized, a) $Sm_2(MoO_4)_3$, b) $Sm_2(MoO_4)_3$/GO c) $Sm_2(MoO_4)_3/C_3N_4$, Tauc's plot for as-prepared, d) $Sm_2(MoO_4)_3$, e) $Sm_2(MoO_4)_3$/GO and f) $Sm_2(MoO_4)_3/C_3N_4$.

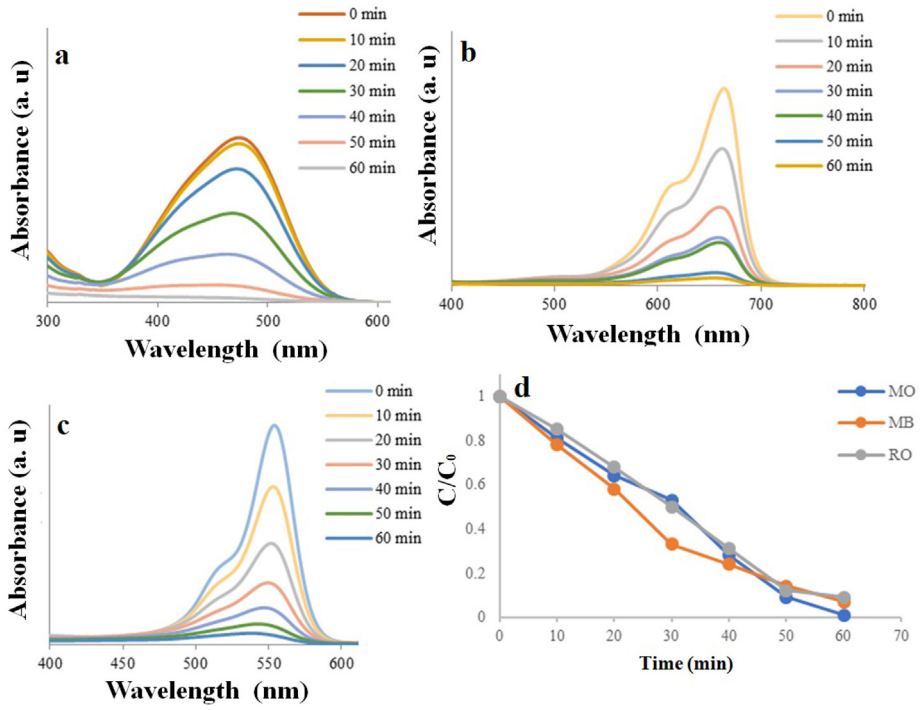

Fig. 7. UV–Vis absorption spectrum of dyes a) methyl orange b) methylene blue, c) rhodamine B in the presence of $Sm_2(MoO_4)_3$ and d) Photocatalytic degradation of different organic dyes by $Sm_2(MoO_4)_3$ under ultraviolet light. (For interpretation of the references to colour in this figure legend, the reader is referred to the web version of this article.)

3.6. Optimal catalyst concentration

The optimal concentration of the catalyst to remove the maximum amount of the pollutants was determined using 0.05, 0.1 and 0.15 g/l of the catalyst. Accordingly 0.025, 0.05 and 0.075 g of the catalyst were separately added to 2 ml distilled water. Each of them was then separately poured into 500 ml of methyl orange solution (5 ppm) and studied under ultraviolet light. Fig. 8 shows the results of studying of the catalyst concentration in the solution. As shown in the figure, 81, 99 and 69% of degradations were obtained with 0.05, 0.1 and 0.15 g/l concentrations for 60 min, and photocatalyst with 0.1 g/l concentration showed the best results in methyl orange removal.

3.7. The effect of pH

The pH of an MO solution containing 0.1 g/l was changed to 3, 7 and 10. Methyl orange solution (5 ppm) was reached to desire pH by hydrochloric acid and sodium hydroxide. 0.1 g/l of $Sm_2(MoO_4)_3$ was weighed and then dispersed to the solution and the photocatalytic activity was investigated by turning on the UV light. Fig. 9 shows the results, indicating the respective degradation percentages of 82, 99, and 72% for pH values of 3, 7, and 10, respectively. Obviously, the faster methyl orange degradation is resulted in the neutral pH.

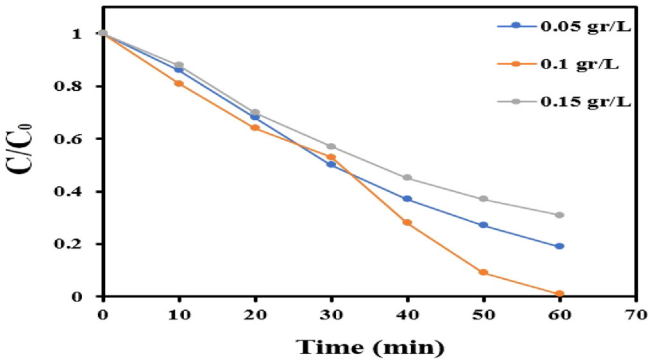

Fig. 8. Photocatalytic degradation of Methyl Orange with different concentrations 0.05, 0.1 and 0.15 g/l of $Sm_2(MoO_4)_3$ as catalyst under UV light. (For interpretation of the references to colour in this figure legend, the reader is referred to the web version of this article.)

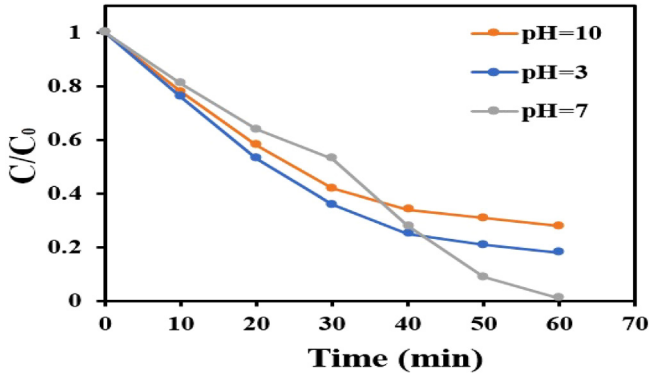

Fig. 9. Photocatalytic degradation of Methyl Orange/ $Sm_2(MoO_4)_3$ (0.1 g/l) at pHs 3, 7 and 10 under UV light.

3.8. The effect of crystallinity

The effect of crystallinity was studied by first calcining of the $Sm_2(MoO_4)_3$ sample at 400 and 800 °C and then the resulting catalyst was used under the optimal conditions determined for the non-calcined sample. According to the results (Fig. 10) higher degradation was observed for non-calcined $Sm_2(MoO_4)_3$.

3.9. Photocatalytic properties of $Sm_2(MoO_4)_3$/GO and $Sm_2(MoO_4)_3$/C_3N_4

The photocatalytic properties of $Sm_2(MoO_4)_3$/GO were evaluated and the results of the UV-induced degradation of MO in the presence of various compositions of this material (1:1, 10:1, and 20:1, $Sm_2(MoO_4)_3$:GO can be seen in Fig. 11a. Based on the results, all composites offer high activities with yields of 92, 97 and 98% for the 1:1, 10:1, and 20:1 catalysts after 50 min, respectively. The $Sm_2(MoO_4)_3/C_3N_4$ composite was also tested and the results in Fig. 10b indicate that for catalysts with $Sm_2(MoO_4)_3$:C_3N_4 ratios of 10: 1 and 30: 1 good photocatalytic activities of 98% and 99% were obtained after 40 min, respectively.

3.10. The reaction kinetics

The studies on $Sm_2(MoO_4)_3$ were performed under the optimal condition of neutral pH and using 0.1 g/l mixture of non-calcined catalyst. The same studies were performed for 20:1 and 30:1 $Sm_2(MoO_4)_3$/GO and $Sm_2(MoO_4)_3/C_3N_4$ composites. The kinetics of the reactions were evaluated in terms of -ln (C/C_0) against time (Fig. 12 a). The results give the slope of the regression line (the pseudo first-order rate constant) with $Sm_2(MoO_4)_3/C_3N_4$ composite offering the maximum relative value. The respective reaction rate constants for $Sm_2(MoO_4)_3$, $Sm_2(MoO_4)_3$/GO, $Sm_2(MoO_4)_3/C_3N_4$ are 0.0524, 0.0811 and 0.1067, respectively. The values of band gap energy, degradation percentage and rate constants under the visible light are shown in table 4. They indicate that $Sm_2(MoO_4)_3$ is the superior species under these conditions. Also, the reaction rate constant under the UV-irradiation for degradation of the MB and Rh B and is shown in Fig. 12b. The value of 0.0429 add 0.0259 for MB and Rh B and respectively, for rate constant of $Sm_2(MoO_4)_3$.

3.11. BET analysis

For the investigation of specific surface area and pore volume, we used BET analysis. The adsorption/desorption isotherm and the JH plots are presented in the Fig. 13 a b and c (without of C_3N_4) and Fig. 13 d, e and f (in the presence of C_3N_4), respectively.

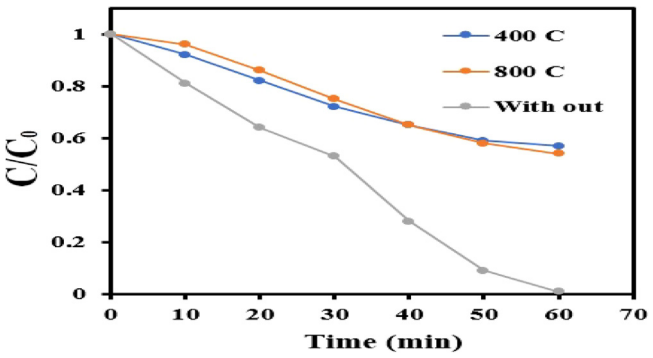

Fig. 10. Photocatalytic degradation of methyl orange at neutral pH with $Sm_2(MoO_4)_3$ (0.1 g/l) calcinated at 400 and 800 °C without calcination.(For interpretation of the references to colour in this figure legend, the reader is referred to the web version of this article.)

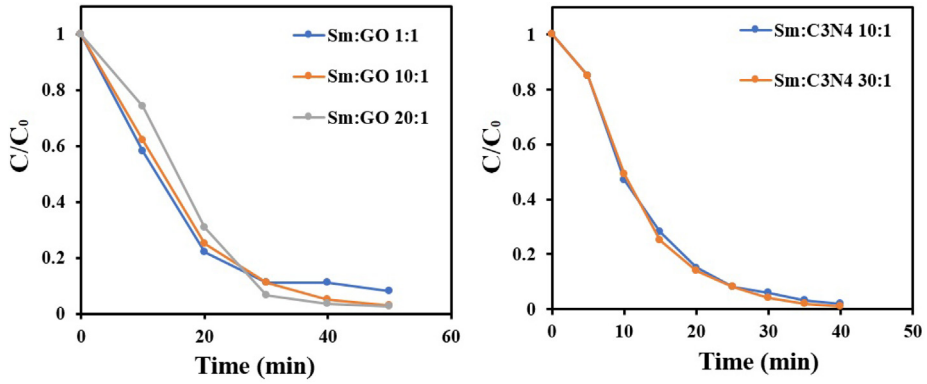

Fig. 11. a) The results of photocatalytic degradation of methyl orange in of 1: 1, 10: 1 and 20: 1 ratio of $Sm_2(MoO_4)_3$/GO b) Results of photocatalytic degradation of methyl orange in 10: 1 and 30: 1 of ratios of $Sm_2(MoO_4)_3/C_3N_4$.(For interpretation of the references to colour in this figure legend, the reader is referred to the web version of this article.)

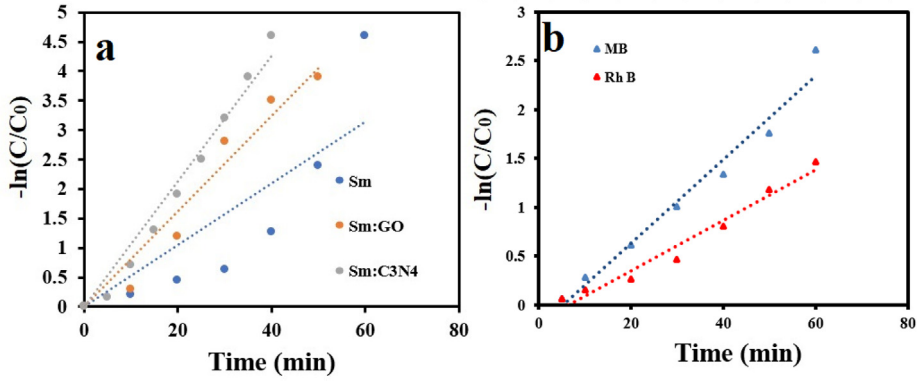

Fig. 12. Pseudo First-order kinetic for degradation of a) MO by $Sm_2(MoO_4)_3$, $Sm_2(MoO_4)_3$/GO nanocomposite and $Sm_2(MoO_4)_3/C_3N_4$ nanocomposite and b) MB and Rh B by $Sm_2(MoO_4)_3$.

Table 4
The optical properties of the $Sm_2(MoO_4)_3$ nanoparticles, $Sm_2(MoO_4)_3$/GO and $Sm_2(MoO_4)_3/C_3N_4$.

Sample No	Band gap values (eV)	Rate constant of MO degradation (h^{-1})	%Degradation of MO
Samarium molybdate	3.75	0.0524	%91
Samarium molybdate/GO	3.15	0.0811	%98
Samarium molybdate/C_3N_4	3.40	0.1067	%99

According to IUPAC's classification, the isotherm of $Sm_2(MoO_4)_3$ reflects a type II isotherm. An explanation for the size of disordered pores for $Sm_2(MoO_4)_3$ nanocomposite prepared in the absence of C_3N_4 has been shown in Fig. 13a. The mean, total pore volumes, and specific surface areas were calculated as 11.89 nm, 0.03167 cm^3/g, and 1.07 m^2/g, respectively. The size dtribution of pores in $Sm_2(MoO_4)_3$ nanocomposite prepared with C_3N_4 has displayed in Fig. 13 c. The mean pore, specific surface areas, total pore volume and diameter for this sample were calculated to be 11.71 nm, 15.787 m^2/g and 0.04623 cm^3/g, respectively. Base on the results, the specific surface area of $Sm_2(MoO_4)_3$ with C_3N_4 increased up to 15 times in comparison without using C_3N_4. This could be led to increased photocatalytic activity of $Sm_2(MoO_4)_3$ nanocomposite prepared with C_3N_4.

3.12. Cytotoxicity effect on MCF-7 cells

The cell viability and cytotoxic effects of the materials against the MCF-7 breast cancer cell were evaluated using MTT assay with various concentrations (16–2000 μg/ml) at two different intervals of incubation (24 and 48 h) as shown in Fig. 14. It was found that the nanoparticles reduced the cell viability and proliferation and this effect increased with the concentration of the materials used. After 24 h of treatment, the inhibitory concentration (IC_{50}) value was ~100, 75. 70 μg/ml for $Sm(MoO_4)$/GO, $Sm(MoO_4)$, $Sm(MoO_4)/C_3N_4$, respectively (Fig. 14 a); but the IC50 of $Sm(MoO_4)$ decreased to ~45 μg/ml and IC50 of $Sm(MoO_4)$/GO, $Sm(MoO_4)/C_3N_4$-10–1 did not show any significant changes after 48 h treatment. It is demonstrated that the morphological features were changed in treated cells nanoparticles which are included in cytoplasmic condensation, increased floating cells, and cell shrinkage in dose dependent manner.

4. Conclusion

Here in, $Sm_2(MoO_4)_3$ nanoparticles were synthesized. To reach the best morphology, different templates were used. Nanostructured $Sm_2(MoO_4)_3$ were prepared and its composite with GO and C_3N_4 were also synthesized. All samples were characterized using SEM, XRD, FTIR and DRS and their particle sizes, compositions and structures were determined. Further, the photocatalytic prop-

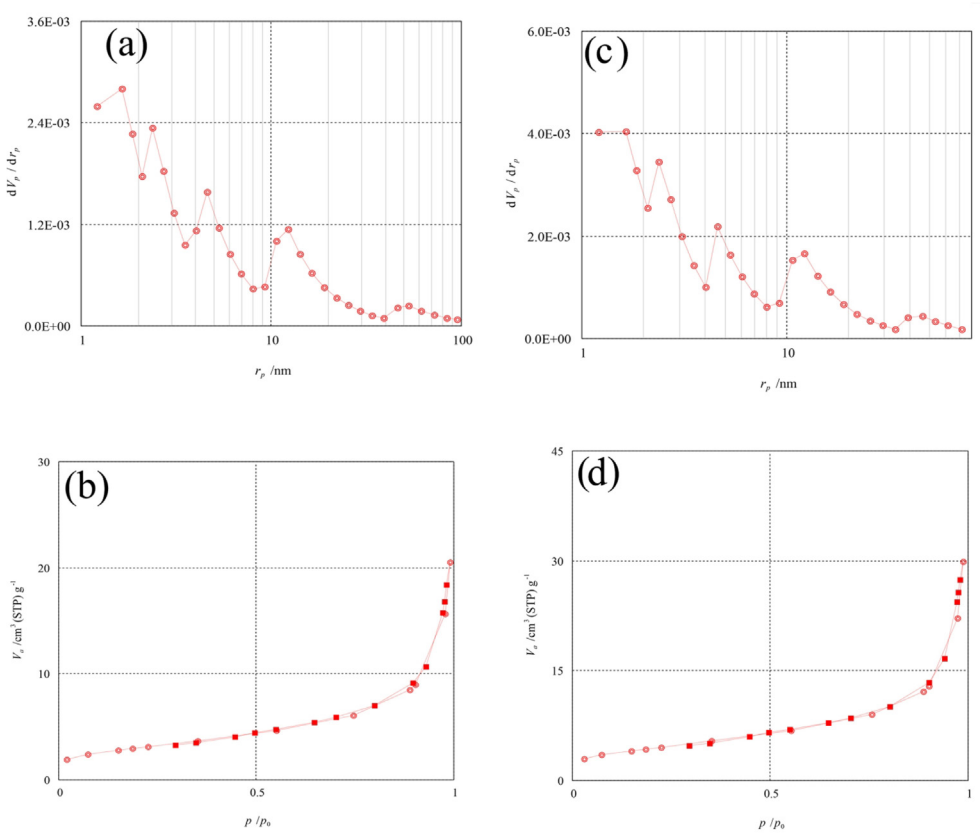

Fig. 13. BET pattern of $Sm_2(MoO_4)_3$ obtained (a,b) without C_3N_4 and (c,d) with C_3N_4.

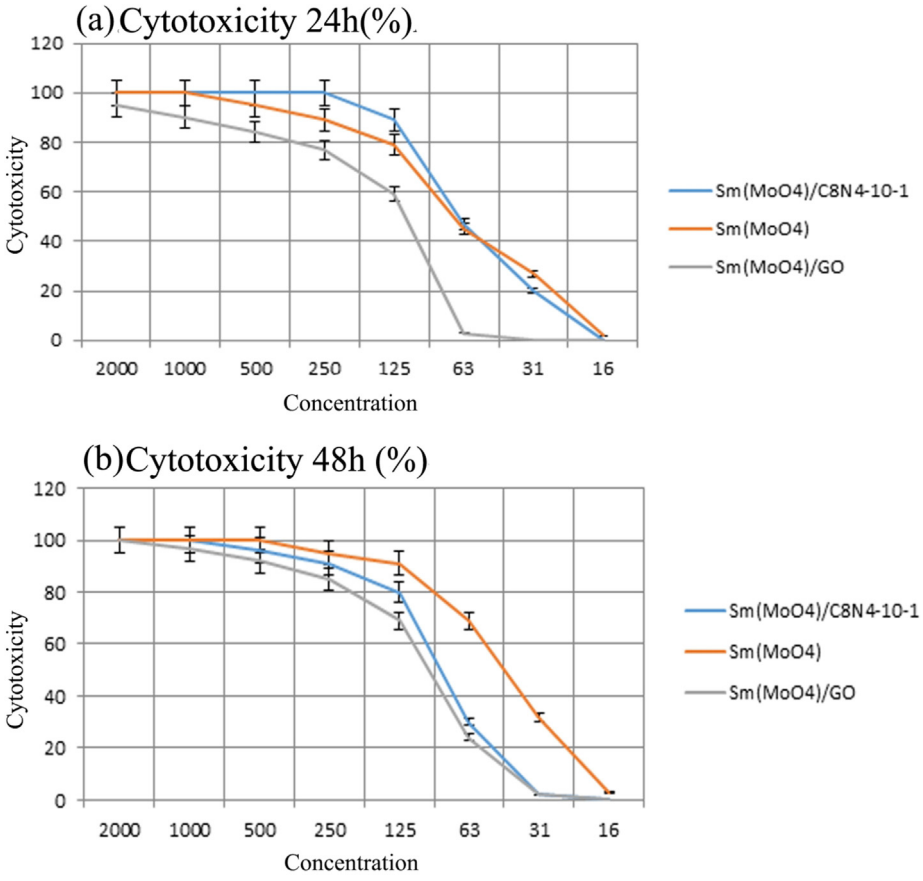

Fig. 14. Relative in vitro cell viability of optimized $Sm_2(MoO_4)_3$, $Sm_2(MoO_4)_3$/GO and $Sm_2(MoO_4)_3/C_3N_4$, MTT assay. MCF-7 cells incubated with samples at different concentration for 24 h (a) and 48 h (b).

erties of the materials were studied and it was found that they can act as powerful photocatalysts to remove organic dyes. The obtained IC50 from MTT assay of the optimum sample in a MCF-7 Cell line was about 125 mg/L.

Author contributions

AS and MR contributed in conception, design, statistical analysis and drafting of the manuscript. SB, MK, HRM, ES, MK, MG and FA contributed in data collection and manuscript drafting. All authors approved the final version for submission

Acknowledgment

We gratefully acknowledge the financial support from Iran University of Medical Sciences, Tehran, Iran, with grant number 50907.

References

[1] J. McLaren, I. Williams, The impact of communicating information about air pollution events on public health, Sci. Total Environ. 538 (2015) 478–491.
[2] W.-K. Jo, R.J. Tayade, New generation energy-efficient light source for photocatalysis: LEDs for environmental applications, Ind. Eng. Chem. Res. 53 (6) (2014) 2073–2084.
[3] T.K. Sen, S. Afroze, H. Ang, Equilibrium, kinetics and mechanism of removal of methylene blue from aqueous solution by adsorption onto pine cone biomass of Pinus radiata, Water Air Soil Pollut. 218 (1–4) (2011) 499–515.
[4] V. Gupta, Application of low-cost adsorbents for dye removal–a review, J. Environ. Manage. 90 (8) (2009) 2313–2342.
[5] N.P. Cheremisinoff, Handbook of water and wastewater treatment technologies, Butterworth-Heinemann, 2001.
[6] S. Avlonitis, I. Poulios, D. Sotiriou, M. Pappas, K. Moutesidis, Simulated cotton dye effluents treatment and reuse by nanofiltration, Desalination 221 (1–3) (2008) 259–267.
[7] S. Cotillas, J. Llanos, P. Cañizares, D. Clematis, G. Cerisola, M.A. Rodrigo, et al., Removal of Procion Red MX-5B dye from wastewater by conductive-diamond electrochemical oxidation, Electrochim. Acta 263 (2018) 1–7.
[8] M.A. Marsooli, M. Fasihi-Ramandi, K. Adib, S. Pourmasoud, F. Ahmadi, M.R. Ganjali, et al., Preparation and Characterization of Magnetic Fe3O4/CdWO4 and Fe3O4/CdWO4/PrVO4 Nanoparticles and Investigation of Their Photocatalytic and Anticancer Properties on PANC1 Cells, Materials. 12 (19) (2019) 3274.
[9] M. Rahimi-Nasrabadi, A. Ghaderi, H.R. Banafshe, M. Eghbali-Arani, M. Akbari, F. Ahmadi, et al., Preparation of Co 2 TiO 4/CoTiO 3/Polyaniline ternary nano-hybrids for enhanced destruction of agriculture poison and organic dyes under visible-light irradiation, J. Mater. Sci.: Mater. Electron. 30 (17) (2019) 15854–15868.
[10] M. Rahimi-Nasrabadi, S.M. Pourmortazavi, M. Aghazadeh, M.R. Ganjali, M.S. Karimi, P. Novrouzi, Optimizing the procedure for the synthesis of nanoscale gadolinium (III) tungstate as efficient photocatalyst, J. Mater. Sci.: Mater. Electron. 28 (4) (2017) 3780–3788.
[11] A. Sobhani-Nasab, S. Behvandi, M.A. Karimi, E. Sohouli, M.S. Karimi, N. Gholipour, et al., Synergetic effect of graphene oxide and C3N4 as co-catalyst for enhanced photocatalytic performance of dyes on Yb2 (MoO4) 3/YbMoO4 nanocomposite, Ceram. Int. (2019).
[12] F. Gandomi, S.M. Peymani-Motlagh, M. Rostami, A. Sobhani-Nasab, M. Fasihi-Ramandi, M. Eghbali-Arani, et al., Simple synthesis and characterization of Li 0.5 Fe 2.5 O4, LiMg0.5Fe2O4 and LiNi0.5Fe2O4, and investigation of their photocatalytic and anticancer properties on hela cells line, J. Mater. Sci.: Mater. Electron. (2019) 1–12.
[13] F.S. Sangsefidi, M. Nejati, J. Verdi, M. Salavati-Niasari, Green synthesis and characterization of cerium oxide nanostructures in the presence carbohydrate sugars as a capping agent and investigation of their cytotoxicity on the mesenchymal stem cell, J. Cleaner Prod. 156 (2017) 741–749.
[14] M. Almessiere, Y. Slimani, M. Sertkol, F. Khan, M. Nawaz, H. Tombuloglu, et al., Ce–Nd Co-substituted nanospinel cobalt ferrites: An investigation of their structural, magnetic, optical, and apoptotic properties, Ceram. Int. (2019).
[15] F. Gandomi, S.M. Peymani-Motlagh, M. Rostami, A. Sobhani-Nasab, M. Fasihi-Ramandi, M. Eghbali-Arani, et al., Simple synthesis and characterization of Li0.5Fe2.5O4, LiMg0.5Fe2O4 and LiNi0.5Fe2O4, and investigation of their photocatalytic and anticancer properties on hela cells line, J. Mater. Sci.: Mater. Electron. 30 (22) (2019) 19691–19702.
[16] S.M. Peymani-Motlagh, A. Sobhani-Nasab, M. Rostami, H. Sobati, M. Eghbali-Arani, M. Fasihi-Ramandi, et al., Assessing the magnetic, cytotoxic and photocatalytic influence of incorporating Yb 3+ or Pr 3+ ions in cobalt–nickel ferrite, J. Mater. Sci.: Mater. Electron. 30 (7) (2019) 6902–6909.
[17] H. Kooshki, A. Sobhani-Nasab, M. Eghbali-Arani, F. Ahmadi, V. Ameri, M. Rahimi-Nasrabadi, Eco-friendly synthesis of PbTiO3 nanoparticles and PbTiO3/carbon quantum dots binary nano-hybrids for enhanced photocatalytic performance under visible light, Sep. Purif. Technol. 211 (2019) 873–881.
[18] A. Sobhani-Nasab, M. Behpour, M. Rahimi-Nasrabadi, F. Ahmadi, S. Pourmasoud, New method for synthesis of BaFe 12 O 19/Sm 2 Ti 2 O 7 and BaFe 12 O 19/Sm 2 Ti 2 O 7/Ag nano-hybrid and investigation of optical and photocatalytic properties, J. Mater. Sci.: Mater. Electron. 30 (6) (2019) 5854–5865.
[19] F. Sedighi, M. Esmaeili-Zare, A. Sobhani-Nasab, M. Behpour, Synthesis and characterization of CuWO 4 nanoparticle and CuWO 4/NiO nanocomposite using co-precipitation method; application in photodegradation of organic dye in water, J. Mater. Sci.: Mater. Electron. 29 (16) (2018) 13737–13745.
[20] S. Zinatloo-Ajabshir, Z. Salehi, M. Salavati-Niasari, Green synthesis of Dy2Ce2O7 ceramic nanostructures using juice of Punica granatum and their efficient application as photocatalytic degradation of organic contaminants under visible light, Ceram. Int. 44 (4) (2018) 3873–3883.
[21] S. Zinatloo-Ajabshir, Z. Salehi, M. Salavati-Niasari, Green synthesis and characterization of Dy2Ce2O7 nanostructures using Ananas comosus with high visible-light photocatalytic activity of organic contaminants, J. Alloy. Compd. 763 (2018) 314–321.
[22] A. Sobhani-Nasab, M. Sadeghi, Preparation and characterization of calcium tungstate nanoparticles with the aid of amino acids and investigation its photocatalytic application, J. Mater. Sci.: Mater. Electron. 27 (8) (2016) 7933–7938.
[23] M. Salavati-Niasari, F. Soofivand, A. Sobhani-Nasab, M. Shakouri-Arani, M. Hamadanian, S. Bagheri, Facile synthesis and characterization of CdTiO 3 nanoparticles by Pechini sol–gel method, J. Mater. Sci.: Mater. Electron. 28 (20) (2017) 14965–14973.
[24] S.S. Hosseinpour-Mashkani, A. Sobhani-Nasab, Investigation the effect of temperature and polymeric capping agents on the size and photocatalytic properties of NdVO 4 nanoparticles, J. Mater. Sci.: Mater. Electron. 28 (21) (2017) 16459–16466.
[25] S. Joshi, V. Garg, J. Saini, K. Kadirvelu, Removal of toulidine blue O dye from aqueous solution by silica-iron oxide nanoparticles, Mater. Focus. 7 (1) (2018) 140–146.
[26] A. Sobhani-Nasab, S. Pourmasoud, F. Ahmadi, M. Wysokowski, T. Jesionowski, H. Ehrlich, et al., Synthesis and characterization of MnWO4/TmVO4 ternary nano-hybrids by an ultrasonic method for enhanced photocatalytic activity in the degradation of organic dyes, Mater. Lett. 238 (2019) 159–162.
[27] K. Adib, Z. Rezvani, M. Rahimi-Nasrabadi, S.M. Pourmortazavi, Statistically optimized synthesis of cadmium tungstate nanoplates for use as a photocatalyst, J. Mater. Sci.: Mater. Electron. 29 (8) (2018) 6377–6387.
[28] S.M. Pourmortazavi, M. Rahimi-Nasrabadi, F. Ahmadi, M.R. Ganjali, CuCO 3 and CuO nanoparticles; facile preparation and evaluation as photocatalysts, J. Mater. Sci.: Mater. Electron. 29 (11) (2018) 9442–9451.
[29] M. Rahimi-Nasrabadi, S.M. Pourmortazavi, M.R. Ganjali, P. Norouzi, Optimizing the synthesis procedure and characterization of terbium (III) tungstate nanoparticles as high performance photocatalysts, J. Mater. Sci.: Mater. Electron. 28 (13) (2017) 9724–9731.
[30] A. Sobhani-Nasab, S.M. Hosseinpour-Mashkani, M. Salavati-Niasari, H. Taqriri, S. Bagheri, K. Saberyan, Synthesis, characterization, and photovoltaic application of NiTiO 3 nanostructures via two-step sol–gel method, J. Mater. Sci.: Mater. Electron. 26 (8) (2015) 5735–5742.
[31] S.M. Hosseinpour-Mashkani, A. Sobhani-Nasab, M. Mehrzad, Controlling the synthesis SrMoO 4 nanostructures and investigation its photocatalyst application, J. Mater. Sci.: Mater. Electron. 27 (6) (2016) 5758–5763.
[32] C. Tian, Q. Zhang, A. Wu, M. Jiang, Z. Liang, B. Jiang, et al., Cost-effective large-scale synthesis of ZnO photocatalyst with excellent performance for dye photodegradation, Chem. Commun. 48 (23) (2012) 2858–2860.
[33] S. Zinatloo-Ajabshir, M. Salavati-Niasari, Z. Zinatloo-Ajabshir, Nd2Zr2O7-Nd2O3 nanocomposites: new facile synthesis, characterization and investigation of photocatalytic behaviour, Mater. Lett. 180 (2016) 27–30.
[34] X. Lang, H. Ji, C. Chen, W. Ma, J. Zhao, Selective formation of imines by aerobic photocatalytic oxidation of amines on TiO2, Angew. Chem. Int. Ed. 50 (17) (2011) 3934–3937.
[35] K. Hashimoto, H. Irie, A. Fujishima, TiO2 photocatalysis: a historical overview and future prospects, Jpn. J. Appl. Phys. 44 (12R) (2005) 8269.
[36] H. Li, X. He, Z. Kang, H. Huang, Y. Liu, J. Liu, et al., Water-soluble fluorescent carbon quantum dots and photocatalyst design, Angew. Chem. Int. Ed. 49 (26) (2010) 4430–4434.
[37] S. Wang, B.Y. Guan, X. Wang, X.W.D. Lou, Formation of hierarchical Co9S8@ZnIn2S4 heterostructured cages as an efficient photocatalyst for hydrogen evolution, J. Am. Chem. Soc. 140 (45) (2018) 15145–15148.
[38] A. Sobhani-Nasab, M. Behpour, Synthesis, characterization, and morphological control of Eu 2 Ti 2 O 7 nanoparticles through green method and its photocatalyst application, J. Mater. Sci.: Mater. Electron. 27 (11) (2016) 11946–11951.
[39] S.M. Hosseinpour-Mashkani, A. Sobhani-Nasab, Green synthesis and characterization of NaEuTi 2 O 6 nanoparticles and its photocatalyst application, J. Mater. Sci.: Mater. Electron. 28 (5) (2017) 4345–4350.
[40] A. Sobhani-Nasab, M. Behpour, Synthesis and characterization of AgO nanostructures by precipitation method and its photocatalyst application, J. Mater. Sci.: Mater. Electron. 27 (2) (2016) 1191–1196.
[41] S. Mortazavi-Derazkola, S. Zinatloo-Ajabshir, M. Salavati-Niasari, Novel simple solvent-less preparation, characterization and degradation of the cationic dye over holmium oxide ceramic nanostructures, Ceram. Int. 41 (8) (2015) 9593–9601.

[42] S. Zinatloo-Ajabshir, M. Salavati-Niasari, Zirconia Nanostructures: Novel Facile Surfactant-Free Preparation and Characterization, Int. J. Appl. Ceram. Technol. 13 (1) (2016) 108–115.
[43] K. Ranjit, I. Willner, S. Bossmann, A. Braun, Lanthanide oxide-doped titanium dioxide photocatalysts: novel photocatalysts for the enhanced degradation of p-chlorophenoxyacetic acid, Environ. Sci. Technol. 35 (7) (2001) 1544–1549.
[44] A. Sobhani-Nasab, M. Behpour, M. Rahimi-Nasrabadi, F. Ahmadi, S. Pourmasoud, F. Sedighi, Preparation, characterization and investigation of sonophotocatalytic activity of thulium titanate/polyaniline nanocomposites in degradation of dyes, Ultrason. Sonochem. 50 (2019) 46–58.
[45] M. Rahimi-Nasrabadi, M. Behpour, A. Sobhani-Nasab, M.R. Jeddy, Nanocrystalline Ce-doped copper ferrite: synthesis, characterization, and its photocatalyst application, J. Mater. Sci.: Mater. Electron. 27 (11) (2016) 11691–11697.
[46] M. Rahimi-Nasrabadi, M. Behpour, A. Sobhani-Nasab, S.M. Hosseinpour-Mashkani, ZnFe 2–x La x O 4 nanostructure: synthesis, characterization, and its magnetic properties, J. Mater. Sci.: Mater. Electron. 26 (12) (2015) 9776–9781.
[47] S.M. Hosseinpour-Mashkani, M. Maddahfar, A. Sobhani-Nasab, Precipitation synthesis, characterization, morphological control, and photocatalyst application of ZnWO 4 nanoparticles, J. Electron. Mater. 45 (7) (2016) 3612–3620.
[48] S.S. Hosseinpour-Mashkani, S.S. Hosseinpour-Mashkani, A. Sobhani-Nasab, Synthesis and characterization of rod-like CaMoO 4 nanostructure via free surfactant sonochemical route and its photocatalytic application, J. Mater. Sci.: Mater. Electron. 27 (5) (2016) 4351–4355.
[49] Z.-Y. Li, M.S. Akhtar, J.H. Kuk, B.-S. Kong, O.-B. Yang, Graphene application as a counter electrode material for dye-sensitized solar cell, Mater. Lett. 86 (2012) 96–99.
[50] P. Zhai, J.A. Isaacs, M.J. Eckelman, Net energy benefits of carbon nanotube applications, Appl. Energy 173 (2016) 624–634.
[51] B. Zhang, F. Kang, J.-M. Tarascon, J.-K. Kim, Recent advances in electrospun carbon nanofibers and their application in electrochemical energy storage, Prog. Mater. Sci. 76 (2016) 319–380.
[52] C. Melios, C.E. Giusca, V. Panchal, O. Kazakova, Water on graphene: review of recent progress. arXiv preprint arXiv:180409518. 2018.
[53] F. Xu, C. Xu, H. Chen, D. Wu, Z. Gao, X. Ma, et al., The synthesis of Bi2S3/2D-Bi2WO6 composite materials with enhanced photocatalytic activities, J. Alloy. Compd. 780 (2019) 634–642.
[54] X. Li, J. Yu, S. Wageh, A.A. Al-Ghamdi, J. Xie, Graphene in photocatalysis: a review, Small 12 (48) (2016) 6640–6696.
[55] C. Lai, M.-M. Wang, G.-M. Zeng, Y.-G. Liu, D.-L. Huang, C. Zhang, et al., Synthesis of surface molecular imprinted TiO2/graphene photocatalyst and its highly efficient photocatalytic degradation of target pollutant under visible light irradiation, Appl. Surf. Sci. 390 (2016) 368–376.
[56] Y. Lin, C. Lu, C. Wei, Microstructure and photocatalytic performance of BiVO4 prepared by hydrothermal method, J. Alloy. Compd. 781 (2019) 56–63.